

High-Resolution MAS NMR Analysis of PI3-SH3 Amyloid Fibrils: Backbone Conformation and Implications for Protofilament Assembly and Structure^{†,‡}

Marvin J. Bayro,[§] Thorsten Maly,[§] Neil R. Birkett,^{||} Cait E. MacPhee,[⊥] Christopher M. Dobson,^{||} and Robert G. Griffin^{*,§}

[§]*Francis Bitter Magnet Laboratory and Department of Chemistry, Massachusetts Institute of Technology, Cambridge, Massachusetts 02139*, ^{||}*Department of Chemistry, University of Cambridge, Lensfield Road, Cambridge CB2 1EW, U.K.*, and [⊥]*SUPA, School of Physics and Astronomy, University of Edinburgh, Edinburgh EH9 3JZ, U.K.*

Received May 28, 2010; Revised Manuscript Received July 26, 2010

ABSTRACT: The SH3 domain of the PI3 kinase (PI3-SH3 or PI3K-SH3) readily aggregates into fibrils in vitro and has served as an important model system in the investigation of the molecular properties and mechanism of formation of amyloid fibrils. We describe the molecular conformation of PI3-SH3 in amyloid fibril form as revealed by magic-angle spinning (MAS) solid-state nuclear magnetic resonance (NMR) spectroscopy. The MAS NMR spectra of these fibrils display excellent resolution, with narrow ¹³C and ¹⁵N line widths, representing a high degree of structural order and the absence of extensive molecular motion for the majority of the polypeptide chain. We have identified the spin systems of 82 of the 86 residues in the protein and obtained sequential resonance assignments for 75 of them. Chemical shift analysis indicates that the protein subunits making up the fibril adopt a compact conformation consisting of four well-defined β -sheet regions and four random-coil elements with varying degrees of local dynamics or disorder. The backbone conformation of PI3-SH3 in fibril form differs significantly from that of the native state of the protein, both in secondary structure and in the location of dynamic or disordered segments. The site-specific MAS NMR analysis of PI3-SH3 fibrils we report here is compared with previously published mechanistic and structural data, resulting in a detailed interpretation of the factors that mediate fibril formation by PI3-SH3 and allowing us to propose a possible model of the core structure of the fibrils. Our results confirm the structural similarities between PI3-SH3 fibrils and amyloid assemblies directly related to degenerative and infectious diseases.

Amyloid fibrils are filamentous structures resulting from the spontaneous self-assembly of otherwise soluble peptides and proteins (1–4). A large number of human disorders, including Alzheimer's and Parkinson's diseases, type 2 diabetes, and a variety of systemic amyloidoses, are associated with the formation of such macromolecular assemblies (1, 5, 6). Under each of these pathological conditions, a specific peptide or protein, or protein fragment, transforms from its usual soluble native form into insoluble amyloid fibrils that can accumulate in a variety of organs and tissues. The manner in which the process of amyloid fibril formation leads to the pathogenic behavior that characterizes these diseases is not yet clear; however, under the systemic conditions, it is likely that the fibrils themselves contribute very significantly to the process of organ damage (5). Furthermore, an increasing number of proteins with no link to deposition diseases have been found to form functional amyloid structures in organisms ranging from bacteria to mammals (7–10).

The mechanisms of amyloid fibril formation, and the structures of the amyloid fibrils themselves, are inherently interesting topics and raise important questions from a physical as well as a

biological perspective (11). To explain the molecular basis of amyloid fibril formation by globular proteins, it has been proposed that a critical early step is the partial unfolding of the protein, resulting in flexible conformers that expose aggregation-prone regions of the sequence, which are largely buried in the native state, to the external environment (12). In the example investigated here, fibrils are formed in vitro by the SH3 domain of the p85 α subunit of bovine phosphatidylinositol 3-kinase (PI3-SH3)¹ under acidic conditions (13). The structure of the protein in its native state is well-characterized by X-ray crystallography (14) and solution NMR spectroscopy (15–17), and studies of the acid-unfolded state provide clear evidence that the protein adopts a partially folded conformation prior to fibril formation (13, 18). However, to understand in detail the mechanism by which PI3-SH3 fibrils form and to characterize their properties, it is necessary to elucidate the structure of the fibrillar state at atomic resolution. In combination with information available from previous biophysical studies of this system, the characterization of PI3-SH3 fibrils is likely to reveal significant insights into the universal features of amyloid formation and structure (19–23).

Proteins that readily aggregate to form amyloid fibrils do not share any obvious sequence identity or structural homology to one another. Prior to their transformation into fibrils,

[†]This work was supported by the National Institutes of Health (Grants EB-003151 and EB-002026) and the Leverhulme and Wellcome Trusts. T.M. thanks the Deutsche Forschungs Gesellschaft (DFG) for a Postdoctoral Fellowship.

[‡]Chemical shifts have been deposited in the Biological Magnetic Resonance Bank (BMRB) as entry 16448.

*To whom correspondence should be addressed: Massachusetts Institute of Technology, 170 Albany St., Cambridge, MA 02139. E-mail: rgg@mit.edu. Telephone: (617) 253-5597. Fax: (617) 253-5404.

¹Abbreviations: CP, cross polarization; CSI, chemical shift index; MAS, magic-angle spinning; PDSD, proton-driven spin diffusion; PI3-SH3, SH3 domain of the p85 α subunit of bovine phosphatidylinositol 3-kinase; RFDR, radiofrequency-driven recoupling; TALOS, torsion angle likelihood obtained from shift and sequence similarity; TEDOR, transferred echo double resonance.

amyloidogenic proteins can possess a variety of secondary structure elements, but in their fibrillar state, as revealed by X-ray fiber diffraction data, they adopt a cross- β structure, in which arrays of β -strands are oriented approximately perpendicular to the long axis of the fibril. In addition, fibrils from a wide variety of peptides and proteins typically display a long, unbranched, and frequently twisted morphology (24), and it increasingly appears that the ability to form fibrils is an inherent property of polypeptide chains and not restricted to pathological cases, although the propensity to aggregate and the molecular details of the resulting structures are highly sequence-dependent (1).

The physical properties of amyloid fibrils impede their study by conventional high-resolution structural techniques such as single-crystal X-ray crystallography and solution NMR spectroscopy. Specifically, they do not possess long-range three-dimensional order, do not diffract to high resolution, are typically insoluble, and have high molecular weights. Therefore, the majority of structural information about these species has been obtained through complementary techniques such as transmission electron microscopy, atomic force microscopy, and X-ray fiber diffraction (24–26). In the past decade, however, significant advances in magic-angle spinning solid-state NMR (MAS NMR), notably dipolar recoupling methodology, have enabled the de novo determination of the structures of complex biological molecules in the solid state. In particular, high-resolution MAS NMR structures have been obtained for short peptides and microcrystalline proteins (27–30) and for an 11-residue fragment of human transthyretin (TTR) in its amyloid fibril form (31, 32). Furthermore, detailed structural information and, in some cases, structural models have been obtained by MAS NMR spectroscopy for several amyloid fibrils and prion proteins such as α -synuclein (33), the amyloid- β (A β) peptide (34–38), the GNNQQNY fragment of Sup35 (39), β_2 -microglobulin (40), HET-s (41), and a fragment of the yeast prion protein Ure2p (42). MAS NMR experiments based on dipole–dipole interactions permit the analysis of rigid structural domains, such as the core of amyloid fibrils. In addition, the incorporation of techniques originally developed for liquid-state NMR studies into MAS NMR experiments (43) facilitates the analysis of highly flexible regions of the fibril (33, 44). Solid-state NMR spectroscopy is therefore a highly versatile method for the study of the structure and dynamics of biological macromolecules, even those as challenging to characterize as amyloid fibrils (45) and other kinds of protein aggregates and assemblies (46–48).

In this article, we describe site-specific structural characteristics of PI3-SH3 in amyloid fibril form determined via MAS NMR spectroscopy. The dipolar correlation spectra of PI3-SH3 exhibit excellent resolution, allowing us to identify 82 spin systems for the 86-residue protein. Analysis of samples prepared with alternating ^{13}C – ^{12}C labeling (28, 49, 50) resulted in site-specific assignments for the majority of the ^{13}C and ^{15}N resonances observed. Spectral and chemical shift analyses suggest that the backbone conformation of PI3-SH3 in fibril form consists of well-defined secondary structure elements interrupted by short segments of less regular structure. Interpreting the results from previous structural and mechanistic studies on PI3-SH3, in light of the molecular conformation of the fibril subunits reported here, provides key insights into the process of fibril formation and overall fibril structure. The amyloid characteristics at the molecular level of PI3-SH3 described here are similar to those of disease-associated protein fibrils and thus strongly support the idea that amyloid fibrils are commonly

accessible structural states (1, 4) and highlight the importance of studying model systems to enhance our understanding of the underlying principles of amyloid assembly and structure.

MATERIALS AND METHODS

Sample Preparation. The 86-residue, 9.6 kDa PI3-SH3 domain was expressed as a His₆ tag fusion construct in BL21-(DE3)pLysS *Escherichia coli* cells using M9 minimal medium as described previously (13). For uniformly ^{13}C - and ^{15}N -labeled material (U-PI3-SH3), the medium was supplemented with [^{15}N]ammonium chloride and [^{13}C]glucose as the sole nitrogen and carbon sources, respectively. A sample in which ^{13}C is incorporated in approximately every other carbon site (2-PI3-SH3) was prepared using [2- ^{13}C]glycerol and NaH $^{13}\text{CO}_3$ (Cambridge Isotopes, Andover, MA) as the sole sources of carbon (28, 49). The protein was isolated by nickel affinity chromatography and further purified by size exclusion chromatography. Fibrils with a long, straight morphology were prepared by incubation of 1.0 mM monomeric PI3-SH3 in aqueous solution at pH 2.0 for 2–3 weeks at 25 °C, and collected from solution by centrifugation. Fibril morphology was verified by transmission electron microscopy (TEM). For MAS NMR experiments, the buffer was changed to a 60/40 (w/w) mixture of *d*₅-glycerol and buffer at pH 2.0, via repeated cycles of centrifugation and resuspension, prior to an ultracentrifugation step for concentration. The waxlike pellet contained approximately 0.5 mg of fibrils/mg of sample material. Finally, the pellet was transferred into a MAS rotor by centrifugation. The samples consisted of approximately 5 and 8 mg of protein packed into 2.5 and 3.2 mm rotors, respectively. A lack of change in fibril morphology after several weeks of MAS NMR data acquisition was verified via TEM images.

MAS NMR Spectroscopy and Data Analysis. NMR experiments were performed on custom-designed spectrometers (courtesy of D. J. Ruben, Francis Bitter Magnet Laboratory) operating at ^1H Larmor frequencies of 700 and 750 MHz. Experiments at 700 MHz were performed using a Varian 3.2 mm triple-resonance probe (Varian Inc., Palo Alto, CA), while at 750 MHz, a Bruker 2.5 mm triple-resonance probe (Bruker BioSpin, Billerica, MA) was used. The sample temperature was maintained by using a stream of nitrogen gas (2 °C). Correlation experiments utilized ramped cross polarization (CP) and two-pulse phase modulation (TPPM) heteronuclear decoupling (51) and were performed at MAS frequencies ($\omega_r/2\pi$) between 10.0 and 28.5 kHz. For homonuclear correlation experiments, RFDR (52–54), DREAM (55), CMAR (56), and PDS (57) mixing schemes were used with U-PI3-SH3, while RFDR, PDS, and BASE RFDR (58) were used with 2-PI3-SH3. CMAR experiments were conducted at $\omega_r/2\pi = 28.571$ kHz using a ^{13}C radiofrequency field of $\omega_1/2\pi = 100.0$ kHz. Broadband RFDR experiments were conducted either at $\omega_r/2\pi = 18.182$ kHz using ^{13}C $\omega_1/2\pi = 40$ kHz and high-power ^1H decoupling or at $\omega_r/2\pi = 28.571$ kHz using ^{13}C $\omega_1/2\pi = 120$ kHz without ^1H decoupling during the mixing time. PDS experiments were conducted at $\omega_r/2\pi = 10$ – 12.5 kHz, with mixing times between 50 and 300 ms. DREAM correlations over the ^{13}C aliphatic ^{13}C region were recorded at $\omega_r/2\pi = 16.667$ and 28.571 kHz. Heteronuclear correlations were obtained using SPECIFIC CP (59) and TEDOR (60–62) experiments (1.6 and 6.0 ms mixing times). Data collection consisted of 1024 indirect points with increments of 25 μs for homonuclear spectra and 320 indirect

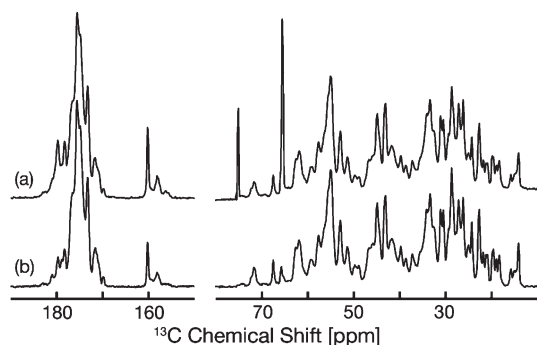


FIGURE 1: 1D ^{13}C MAS NMR spectra of U-PI3-SH3 fibrils recorded at a 750 MHz ^1H Larmor frequency and $\omega_r/2\pi = 16.67$ kHz, at 2 °C. (a) Direct ^{13}C spectrum (Bloch decay), scaled by a factor of 2.5. (b) ^{13}C cross polarization spectrum obtained with a contact time of 1.5 ms.

points with increments of 80 μs for heteronuclear spectra. DREAM, CMAR, RFDR, and 1.6 ms TEDOR spectra were averaged for approximately 48 h each, while PDSO, BASE RFDR, NCXY, and 6 ms TEDOR spectra were averaged for 4–5 days each. ^{13}C and ^{15}N chemical shifts were indirectly referenced to DSS (63) and liquid ammonia (64), respectively. NMR data were processed using NMRPipe (65) and analyzed with Sparky (T. D. Goddard and D. G. Kneller, SPARKY 3, University of California, San Francisco). Secondary structure elements were predicted by calculating chemical shift deviations from random-coil values (66) using the secondary shift values listed by Zhang et al. (67). Backbone torsion angles ϕ and ψ were predicted with TALOS (68), version 2007.068.09.07.

RESULTS

Fibril Homogeneity and Spectral Quality. Amyloid fibrils formed by PI3-SH3 adopt preferentially a single morphology and are remarkably stable (23). No signals from monomeric PI3-SH3 were observed in MAS NMR spectra. Furthermore, the five samples employed in our analysis show exclusively a single set of chemical shifts, and no significant variations in resonance positions were evident among the five different preparations. A second form, uniquely observed in a sixth sample, showed spectral differences from the first form generated under apparently identical conditions but was not pursued further in this study, which focuses solely on the first, dominant form.

One-dimensional (1D) MAS NMR spectra of PI3-SH3 fibrils are of very high resolution and permit the observation of important structural features. Two spectra of uniformly labeled PI3-SH3 (U-PI3-SH3) are shown in Figure 1, a directly detected ^{13}C MAS spectrum (top) and a ^1H – ^{13}C CP MAS spectrum (bottom). These two spectra are remarkably similar to each other in most of their salient features, the only exception being slightly different intensities for a small number of side-chain resonances. This finding indicates that the protein backbone in PI3-SH3 is in a well-defined conformation such that CP enhancement is essentially uniform throughout the polypeptide chain. Indeed, MAS NMR spectra of PI3-SH3 utilizing the INEPT method, aimed at selectively exciting ^{13}C sites in highly flexible regions, yield no protein signals in the temperature range explored in these studies (–10 to 25 °C). CP spectra at various temperatures are shown in Figure S1 of the Supporting Information. The absence of highly mobile carbon sites, and the high degree of similarity between the CP and the direct ^{13}C polarization spectra, indicate that the majority of the PI3-SH3 polypeptide chain adopts a very rigid

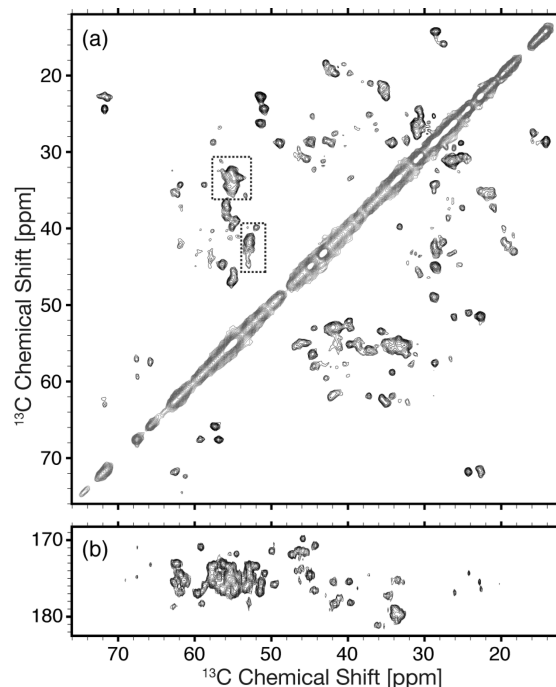


FIGURE 2: 2D ^{13}C – ^{13}C correlation spectra of U-PI3-SH3 (750 MHz ^1H Larmor frequency, at 2 °C). (a) Aliphatic region of a CMAR spectrum (2 ms mixing time, $\omega_r/2\pi = 28.571$ kHz). Areas with a high degree of spectral overlap are indicated. (b) Carbonyl–aliphatic region of RFDR (1.76 ms mixing time, $\omega_r/2\pi = 18.182$ kHz).

conformation in its fibrillar state, in contrast to observations for several other fibrillar systems studied recently, such as α -synuclein (33), Het-s (44), and a human prion protein (69), where the constituent protein subunits are observed to have both rigid and mobile segments.

A very high degree of structural homogeneity is clearly evident from the two-dimensional (2D) ^{13}C – ^{13}C correlation spectra of U-PI3-SH3, as illustrated in Figures 2 and 3. The average ^{13}C line width is less than 0.5 ppm (94 Hz at a ^1H Larmor frequency of 750 MHz), comparable to that observed in uniformly labeled microcrystalline proteins (28, 29, 70–72). Because the spectral resolution of fibril samples depends on their hydration levels (73), we dispersed PI3-SH3 fibrils in a glycerol/water mixture (60/40, w/w) prior to recording spectra to inhibit dehydration of the samples by exploiting the low vapor pressure and hygroscopic properties of glycerol. Indeed, MAS NMR spectra of PI3-SH3 fibrils in buffer alone (pH 2.0) show considerably larger line widths under the same experimental conditions compared to those of fibrils in the glycerol/water mixture described above (Figure S2 of the Supporting Information), while the chemical shifts show only marginal changes. Besides preventing dehydration, it is also possible that the glycerol solvent, which has a stabilizing effect on protein structures, may restrict motion in the fibrils and thus contribute to increased structural order and result in narrower lines.

MAS NMR spectra with a resolution comparable to the resolution of those reported here have been observed for a number of amyloid systems, including the TTR fragment mentioned above (31) and the prion protein fragment HET-s (41). However, in other cases, the observed line widths for amyloid fibrils observed in MAS NMR spectra typically vary between 1 and 5 ppm (33, 34, 39, 74). The excellent quality of the dipolar correlation spectra of U-PI3-SH3 is therefore noteworthy and can be attributed at least in part to careful control of experimental

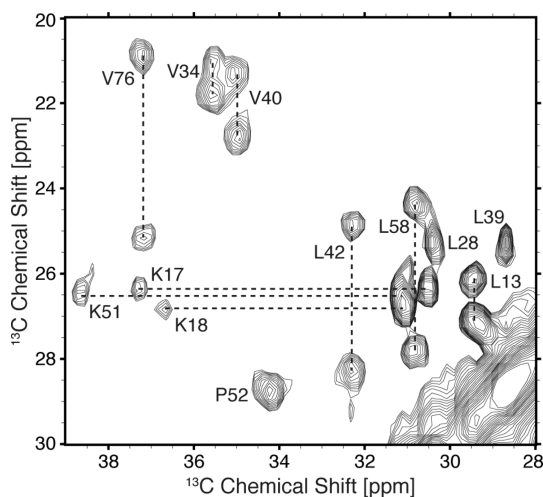


FIGURE 3: Section of a 2D ^{13}C – ^{13}C RFDR (1.76 ms) spectrum of U-PI3-SH3 illustrating aliphatic side-chain correlations, recorded at a 750 MHz ^1H Larmor frequency, 2 °C, and $\omega_r/2\pi = 18.182$ kHz. Typical line widths are between 80 and 115 Hz (0.4–0.6 ppm).

conditions but is also indicative of the inherent homogeneity of PI3-SH3 fibrils at the molecular level.

Despite the narrow line widths characteristic of PI3-SH3 fibrils, certain regions of the correlation spectra show a significant degree of resonance overlap consistent with localized structural degeneracy. For example, aliphatic ^{13}C – ^{13}C correlation spectra exhibit extensive overlap of $^{13}\text{C}\alpha$ – $^{13}\text{C}\beta$ cross-peaks at chemical shift positions typical of Glu/Gln and Asp/Asn residues (marked with boxes in Figure 2). A low degree of chemical shift dispersion is a consequence of limited variability in secondary structure and thus is likely to be a feature of the spectra of amyloid fibrils as a result of their high β -sheet content. However, it could also be a consequence of a small degree of local disorder.

Site-Specific Resonance Assignments of PI3-SH3 Amyloid Fibrils. Using a combination of 2D homonuclear dipolar correlation experiments with short mixing periods (Figures 2 and 3 and Figure S3 of the Supporting Information), it was possible to identify 82 ^{13}C spin systems of a total of 86 residues, and all the side-chain resonances are observed for the majority of spin systems. A number of sequential connectivities were initially established with heteronuclear NCACX and NCOCX experiments (59) and with homonuclear ^{13}C – ^{13}C correlation experiments under weak coupling conditions (75) using the U-PI3-SH3 sample. However, to complement and expedite spectral analysis, we exploited the improved resolution of the 2-PI3-SH3 sample relative to the uniformly labeled one, as well as its characteristic attenuation of dipolar truncation effects (76). Spectra of 2-PI3-SH3 typically exhibit ^{13}C line widths of <0.2 ppm (~ 38 Hz, at a ^1H frequency of 750 MHz) for positions without an adjacent ^{13}C label and line widths of <0.1 ppm (~ 19 Hz, at a ^1H frequency of 750 MHz) for some side-chain resonances.

Sequential inter-residue correlations in 2-PI3-SH3 were established using band-selective radiofrequency dipolar recoupling (BASE RFDR) experiments optimized for aliphatic ^{13}C nuclei and RFDR for broadband carbonyl–aliphatic recoupling. BASE RFDR generates highly sensitive sequential correlations between aliphatic nuclei, as described recently (58). In particular, a large number of $^{13}\text{C}\alpha(i)$ – $^{13}\text{C}\alpha(i \pm 1)$ and $^{13}\text{C}\alpha(i)$ – $^{13}\text{C}\beta(i \pm 1)$ correlations appear readily in BASE RFDR spectra of 2-PI3-SH3, which greatly facilitates resonance assignment. A broadband

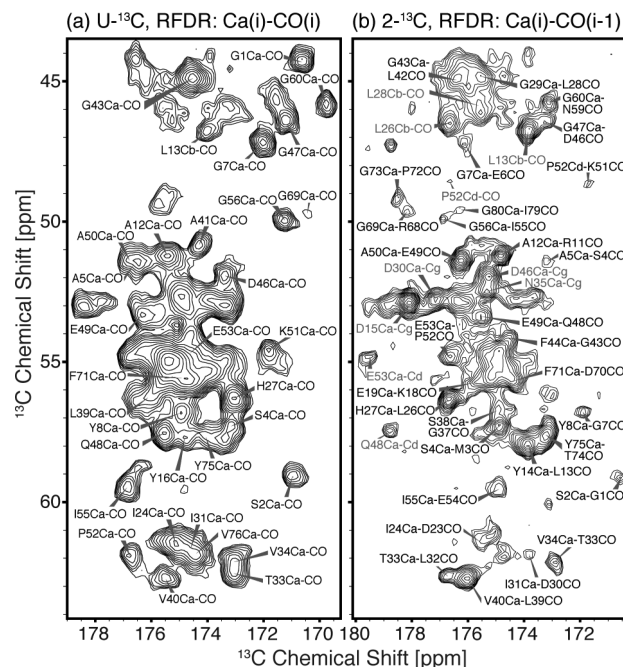


FIGURE 4: Comparison of cross-pick information that can be attained in broadband $\text{C}\alpha$ – C' correlation spectra of U-PI3-SH3 and 2-PI3-SH3. (a) $\text{C}\alpha$ – C' region of a U-PI3-SH3 spectrum recorded with RFDR with a 2.24 ms mixing time, displaying intraresidue one-bond correlations, some of which are labeled. (b) Similar region of a 2-PI3-SH3 spectrum recorded with RFDR with a 6.72 ms mixing time, presenting multiple inter-residue two-bond correlations, labeled in black, and two-bond intraresidue correlations, labeled in gray. Both spectra were recorded at $\omega_r/2\pi = 28.571$ kHz employing $\omega_1/2\pi = 120$ kHz ^{13}C π pulses without ^1H decoupling during the mixing period.

RFDR experiment, optimized for two-bond $^{13}\text{C}'(i)$ – $^{13}\text{C}\alpha(i+1)$ pairs, can also yield highly informative sequential cross-peaks. Figure 4 compares the resonance assignment information available in broadband RFDR experiments with U-PI3-SH3 and 2-PI3-SH3. Both spectra were recorded under similar conditions (17.6 T and $\omega_r/2\pi = 28.5$ kHz) using RFDR mixing without ^1H decoupling and optimized for one-bond transfer (U-PI3-SH3) and two-bond transfer (2-PI3-SH3). Generation and identification of two-bond $^{13}\text{C}'(i)$ – $^{13}\text{C}\alpha(i+1)$ cross-peaks in U-PI3-SH3 at longer mixing times are precluded by dipolar truncation and by overlap with one-bond intraresidue $^{13}\text{C}'(i)$ – $^{13}\text{C}\alpha(i)$ cross-peaks, respectively. There are few of the latter in 2-PI3-SH3, and thus numerous sequential correlations may be identified, provided that both ^{13}C sites are labeled simultaneously by this alternating labeling scheme, in at least a fraction of the protein sample. PDSD experiments with 200–300 ms mixing times, although less efficient, provide additional corroboration of homonuclear sequential connectivities obtained with BASE RFDR and two-bond RFDR.

Heteronuclear sequential correlations were obtained with TEDOR experiments on 2-PI3-SH3, optimized for either one-bond or two-bond mixing. The latter provided numerous $^{15}\text{N}(i)$ – $^{13}\text{C}(i-1)$ connectivities that aided the assignment process and corroborated the partial NCXCY assignments obtained with U-PI3-SH3. Figure 5 illustrates several examples of these sequential TEDOR correlations obtained with 2-PI3-SH3. Because of the improved resolution afforded by this sample, multiple $^{15}\text{N}(i)$ – $^{13}\text{C}\alpha(i-1)$ cross-peaks can be resolved and used to expand upon and verify homonuclear sequential correlations. A detailed description of our resonance assignment scheme and analysis of 2D sequential correlations in samples

labeled with $[2-^{13}\text{C}]$ glycerol will be the subject of a forthcoming publication.

Site-specific resonance assignments were elucidated for 75 residues, located in two large stretches (G1–K18 and L25–G80) of the sequence, thus leaving two small segments of the sequence unassigned, E19–I24 and the C-terminus, R81–S85, with the exception of P86, assigned unambiguously by elimination. Figure 6a shows the amino acid sequence of PI3-SH3, highlighting the

residues that have been assigned at least in part. ^{13}C and ^{15}N chemical shifts for all assigned nuclei are provided in Table 1 of the Supporting Information.

For several spin systems identified in ^{13}C – ^{13}C dipolar correlation spectra of U-PI3-SH3, it was not possible to establish inter-residue connections in either U-PI3-SH3 or 2-PI3-SH3 samples because of the severe overlap of backbone resonances. In some cases, spin systems were ambiguously identified through their characteristic ^{13}C – ^{13}C correlations but did not yield sequential connectivities with sufficient certainty to establish unambiguous assignments.

Secondary Structure and Dynamics. Site-specific analysis of the MAS NMR spectra allows us to elucidate both global and local characteristics of the PI3-SH3 fibril structure. The well-resolved spectra, presenting a unique set of resonances, are consistent with a high degree of structural homogeneity throughout the fibrils, with every residue in the sequence being in a single environment within the fibril. Secondary structure elements were predicted from the difference between the observed ^{13}C and ^{15}N chemical shifts and their random-coil values, using the chemical shift index (66, 67, 77). Here, the quantity $\Delta\delta = \delta^{13}\text{C}\alpha - \delta^{13}\text{C}\beta$, from ref 77, is particularly useful, because the accuracy of the chemical shifts obtained by MAS NMR experiments is usually lower than those measured in solution NMR experiments. The results are summarized in Figure 6b and suggest that most residues in the well-ordered segments of the polypeptide chain are in a β -strand conformation (see Figure S6 of the Supporting Information for individual secondary shifts). To supplement these results, backbone torsion angles φ and ψ were predicted from the chemical shifts using TALOS (68), as shown in Figure 6c (see Figure S7 of the Supporting Information for further details). The results from this database approach agree closely with the secondary structure predictions from the chemical shift index.

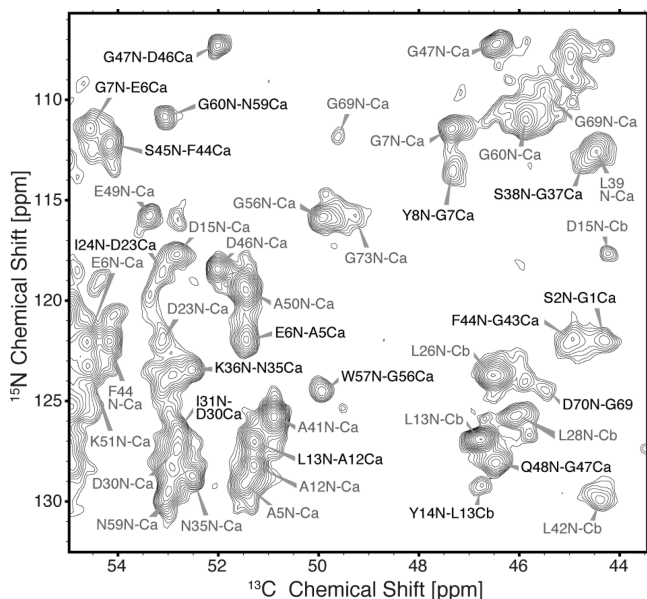


FIGURE 5: Section of a TEDOR spectrum of 2-PI3-SH3 optimized for two-bond ^{15}N – ^{13}C transfer with a 6 ms mixing period, recorded at $\omega_r/2\pi = 10$ kHz and a 700 MHz ^1H Larmor frequency. Sequential correlations are labeled in black and intraresidue cross-peaks in gray.

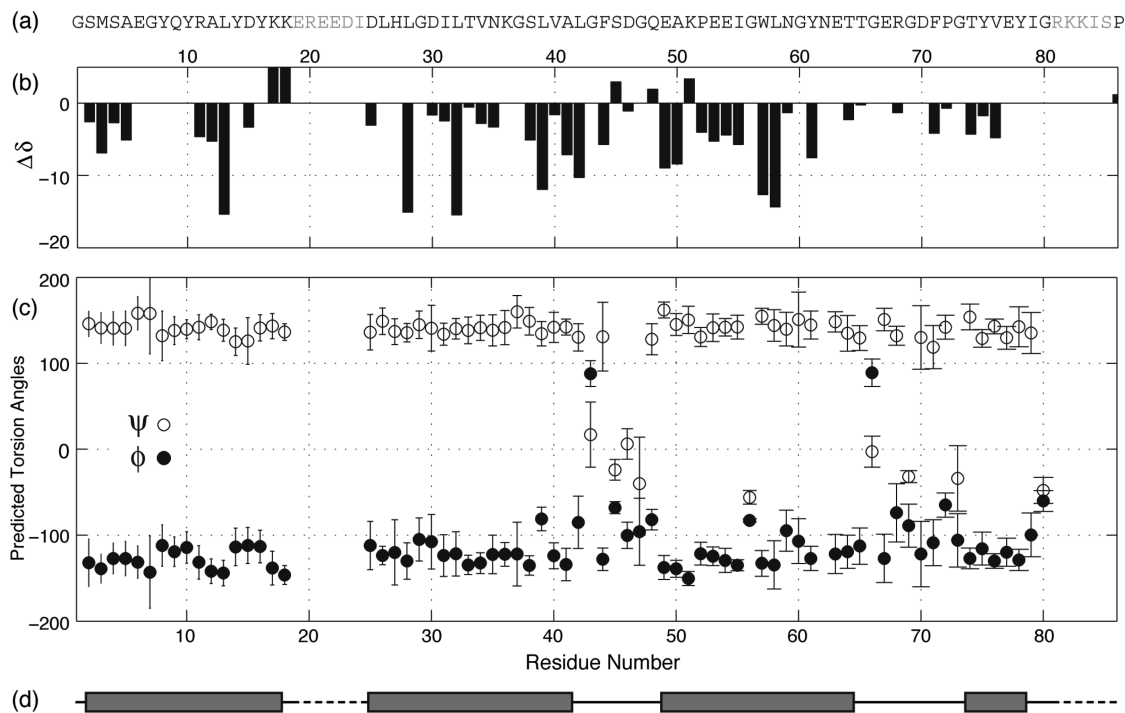


FIGURE 6: Chemical shift analysis. (a) PI3-SH3 sequence, displaying unambiguously assigned (black) and unassigned (gray) residues. (b) Secondary structure propensity derived from the chemical shift index, where negative numbers indicate a β -sheet conformation. (c) Backbone torsion angles (φ and ψ) predicted from ^{13}C and ^{15}N chemical shift analysis using TALOS. (d) Secondary structure diagram of the PI3-SH3 polypeptide chain in amyloid fibril form. Gray bars indicate regions of high β -sheet content, while a single line indicates a random-coil conformation. Dashed lines mark the positions of dynamic/disordered residues.

The secondary structure of PI3-SH3 in its amyloid fibril state consists of four well-defined segments adopting predominantly β -strand conformations, linked by random-coil elements. Chemical shift analysis indicates that three long stretches of residues assume torsion angles consistent with a β -strand secondary structure, namely, S2–K17, L26–A41, and E49–T64, in addition to a short fourth segment, T74–Y78. It is important to point out that these predictions may be ambiguous, particularly for segments including glycine residues, and additional tertiary constraints are needed to define the location and structure of β -sheets accurately. The residues that connect the first and second β -strand regions (E19–I24) present weak backbone and side-chain signals in MAS NMR spectra, and thus, most of them have not been assigned unambiguously. However, on the basis of such spectral characteristics, we can speculate that this small region of the sequence is not well-defined structurally, presenting either dynamic disorder or conformational heterogeneity. The same conclusions can be reached regarding the last six residues of the sequence. On the other hand, the sequence of residues (L42–Q48) between the second and third β -strand regions appears to be a well-structured loop, based on their intense and narrow MAS NMR signals with near random-coil chemical shifts. Another region showing near random-coil chemical shifts (T65–G73) is observed between the third and fourth β -strand elements. In summary, the majority of residues giving rise to narrow lines in the MAS NMR spectra of PI3-SH3 fibrils appear to be located in β -strands or in relatively short and ordered regions that link these secondary structure elements.

From the absence of any signals that can be detected by solution-like NMR methods, we can conclude that there are no highly flexible regions in the protein backbone of PI3-SH3 in its fibrillar form. In addition to indicating an overall high level of structural homogeneity, the observation of narrow line widths for the majority of the PI3-SH3 residues when in the fibril state points to the absence of significant dynamic processes on the time scale of the radiofrequency irradiation (decoupling and cross polarization) for these residues, which can lead to line broadening and a loss of intensity in MAS NMR spectra (78, 79). On the other hand, no resonances could be identified for a few residues within the unassigned segments mentioned above, suggesting that such residues could be in regions of the fibril presenting conformational heterogeneity or undergoing local motions on time scales that interfere with the MAS NMR experiments. Such dynamic interference effects could, in principle, be identified through variable temperature experiments over a wide range of temperatures, and such experiments will be reported in future studies. The C-terminal segment of residues I79–S85, part of which presents weak signals in our spectra, is more exposed to the solvent than the rest of the sequence according to H/D exchange data (80). Other residues showing exchange include K36, G37, and S38 and G66 and E67, possibly due to mobility or to their particular structure. Residues G66 and E67 appear to be in random-coil conformations, and while K36, G37, and S38 are part of a β -strand, they may form a bulge exposing their amide protons to the solvent or may be flexible sites due to the presence of glycine residues. The low intensity of the side-chain resonances of K36 may be evidence of the latter.

DISCUSSION

Comparison with the Native Fold. The native structure of PI3-SH3 is composed of five β -strands forming a β -barrel and a

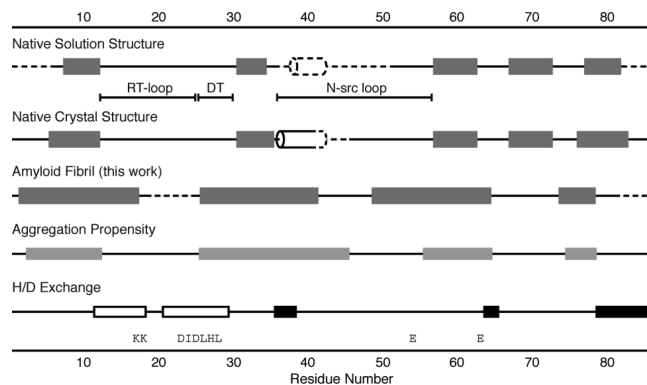


FIGURE 7: Secondary structure of PI3-SH3 amyloid fibrils in the context of previous structural and mechanistic studies. Secondary structure of natively folded PI3-SH3 in solution (15, 16) and in crystalline form (14), with flexible regions shown with dashed lines, and the RT loop, DT, and N-src loop, discussed in the text, marked. Secondary structure of PI3-SH3 in fibril form (from Figure 6d). Aggregation propensity of the PI3-SH3 amino acid sequence (75). H/D exchange results showing highly protected regions (white rectangles) and unprotected sites (black rectangles). A few specific residues discussed in the text are also shown.

short helixlike turn (14–16). Fiber diffraction studies suggest that the orientation of the β -strands in PI3-SH3 fibrils is perpendicular to the fibril axis (13, 81), a finding inconsistent with the β -barrel architecture of the native fold. Nevertheless, a simple rearrangement of the β -strands in the native PI3-SH3 fold could in principle satisfy the above observation and be consistent with electron density maps from cryo-EM image reconstruction studies. A comparison of the secondary structure elements of the native PI3-SH3 fold, previously obtained with solution NMR and X-ray crystallography, to those derived from our solid-state NMR chemical shift analysis is depicted in Figure 7, in which bars and cylinders denote β -sheet and helical segments, respectively, and dashed lines highlight flexible or disordered regions. These plots show that the secondary structure elements identified here for the protein in the fibrillar state are significantly different from those in the native fold. The MAS NMR data show that none of the assigned residues adopt α -helical or helixlike conformations in the fibrils, a finding that is in accordance with circular dichroism and FT-IR data (19). More remarkably, β -strand segments are considerably longer in the fibrils than in the native fold.

The secondary structure elements in the native structure of PI3-SH3, as determined by solution NMR spectroscopy (15, 16), consist of five β -strands, which are four to six residues in length, and short helical segments. In the native PI3-SH3 fold, the first six N-terminal residues are disordered and the first β -strand is formed by Q9–A12, which is followed by a long random-coil segment that includes the RT loop (L13–D25) and the diverging turn (L26–D30). The second β -strand consists of residues I31–V34 and is followed by a flexible stretch of ~ 22 residues in a random-coil conformation (termed the N-src loop), including a short helical segment and a solvent-exposed helical turn (K51–E54). A well-defined type I β -turn (E63–G66) links the third and fourth β -strands, composed of residues W57–N62 and E67–P72, respectively. The fifth β -strand, formed by residues E77–R81, comes after a short helixlike turn and is followed by a disordered C-terminus (K82–P86). A very similar native conformation is found in the crystal structure of PI3-SH3, with the major difference being that, as a result of intermolecular packing, the N-src loop and the C-terminus are less flexible and better defined in the crystal structure (14). In turn, these intermolecular

interactions in the crystal lattice appear to stabilize the secondary structure elements of native PI3-SH3, whose β -strands are longer by a few residues in the crystal structure than in the solution structure, as shown in Figure 7.

Considering the secondary structure elements in the fibrillar state described in the preceding section, we may highlight the following differences (and a few similarities) between PI3-SH3 fibril subunits and the native fold. Three of the five native β -strands are preserved in the fibril state, as part of longer β -strand elements, while residues that form part of β -strands 4 and 5 in the native state (near the C-terminus) adopt mostly a random-coil conformation in the fibril. The natively disordered N-terminus adopts a rigid β -strand structure in the fibril state, while the diverging turn in the native structure changes from a well-defined loop conformation to a β -strand configuration. Similar changes occur for the natively flexible N-src loop region, which encompasses both helical and random-coil residues in the native fold but constitutes the middle of a long, rigid strand-loop-strand region in the fibril state, as shown in Figure 6d. On the other hand, the C-terminal residues, highly flexible in the solution structure, appear also to be dynamically and structurally disordered in the fibrils. Finally, the natively random-coil RT loop constitutes, in the fibril state, both part of a rigid β -strand region (toward the N-terminus) and a disordered segment with few observed MAS NMR signals (towards the C-terminus).

Our observations therefore demonstrate that PI3-SH3 subunits in amyloid fibrils adopt a conformation that is vastly different from that of the native structure of the protein. While fibril measurements by X-ray and cryo-EM (20) can be rationalized with changes in the relative location of secondary structure elements, our data indicate that, in the case of PI3-SH3, only a few residues preserve their conformations between the native state and the fibril state, while the majority of the sequence presents important differences in secondary structure and/or dynamics between one state and the other. This conclusion is consistent with the very different factors that stabilize protein structures in their two alternative highly ordered forms, the native and amyloid states (1, 6).

Aggregation Propensity and Fibril Conformation. PI3-SH3 has been thoroughly studied as a model for the characterization of amyloid fibril formation by a natively globular protein, starting from the acid-unfolded state. In particular, multiple studies have shed light on this protein's propensity to form fibrils as a function of its amino acid sequence and variants thereof, which has led to the identification of key positions in the sequence in which amino acid substitutions may either disrupt or accelerate the aggregation of monomers into amyloid fibrils, as well as segments that have little effect on fibril formation. For example, preparation of chimeras between PI3-SH3 and spectrin-SH3 (SPC-SH3), a structurally homologous protein that does not form fibrils under conditions studied so far, showed that the N-src loop does not have an effect on the aggregation propensity of either protein (82), even though it is the most dissimilar region between the two native structures, being much longer and flexible in PI3-SH3. On the other hand, a short segment from the RT loop and diverging turn regions of PI3-SH3, D23–L28, was sufficient to confer a SPC-SH3 chimera the ability to form amyloid fibrils, suggesting that this part of the sequence of PI3-SH3 has a specific role in its aggregation ability (83). Additional sets of mutations containing at least one residue in this segment were investigated with the aim of exploring the dependence of PI3-SH3 aggregation on three key physicochemical characteristics of polypeptides,

charge, hydrophobicity, and secondary structure tendency (84). The incorporation of extra charges (at pH 2.0) in this region effectively precluded the formation of aggregates, while increasing the polypeptide's helical propensity had a moderate but noticeable effect on discouraging fibril formation (83). Placing charges in regions of the sequence other than the RT loop–DT segment can also have dramatic effects. As reported recently (85), E54K and E63K single mutants have elongation rates several orders of magnitude slower than that of wild-type PI3-SH3, starting with preformed fibrils. These two sites, as well as the RT loop–DT segment, are located near residue stretches that are found to be prone to aggregation, as calculated by the Zyggregator algorithm (86, 87), to which their strong influence has been attributed. Moreover, mutation of a charged residue to a neutral one at pH 2.0 (K18Q) resulted in a 2-fold increase in the rate of elongation of preformed fibrils (85). On the other hand, inserting multiple charges at the N-terminus (via a His tag) did not interfere significantly with PI3-SH3 aggregation (83), further illustrating the sequence dependence of the factors influencing fibril formation by proteins.

Knowing the secondary structure that the PI3-SH3 polypeptide adopts in fibril form, we can discuss the previously published results described above in the context of both aggregation propensity of the amino acid sequence and the final fibril conformation, which are compared in Figure 7. The RT loop–DT segment of residues D23–L28 is at the edge of a β -sheet in the fibril conformation that coincides well with a predicted aggregation-prone region in the unfolded state of PI3-SH3 at pH 2.0 (85), which may explain its fundamental role in fibril formation. Conversely, mutated residues near the aggregation-prone segments, such as L28K and D25R (83), may act as “gatekeepers” that prevent intermolecular association and formation of ordered β -sheets via electrostatic charges (88, 89). Similarly, residues E54 and E63 flank a predicted aggregation-prone region and, moreover, adopt a β -sheet conformation in the final fibril state, as part of a β -strand spanning residues 49–64. The relative location of these residues within the fibril β -strand, with E63 being more peripheral, may account for the slower elongation rate of the E54K mutant compared to that of E63K fibrils (85), while both are orders of magnitude slower than the wild-type case. A different situation is observed for residues K17 and K18, which are distant from calculated aggregation-prone regions and are not effective gatekeepers, even though they end up being adjacent to a β -sheet segment in the fibril state. These observations support the hypothesis that gatekeeper residues can be found in the proximity of calculated aggregation-prone regions in native or unfolded states and are not restricted to positions within β -sheet segments in the mature fibril state. Indeed, several charged residues are incorporated in the highly ordered β -sheets of the fibril conformation of wild-type PI3-SH3 illustrated in Figure 6. Therefore, the ability of charged residues (and additional charges) to disrupt the aggregation process is highly dependent on their position in the sequence, and not only on the conformation they adopt in the fibril state, which may reflect the specific role they play in the assembly mechanism.

Mechanism of PI3-SH3 Fibril Formation. It is interesting to compare our results to published work that addresses directly the mechanism of fibril formation by PI3-SH3. A recent study (80) has shown, via a pulse-labeling hydrogen–deuterium (H/D) exchange technique, that segments A12–K18 and E21–G29 are the most protected from exchange in mature fibrils formed at pH 2.0, which we have analyzed here. A similar region,

Y14–I24, is the most protected in the prefibrillar aggregates observed at pH 1.5, a condition found to favor the stabilization of PI3-SH3 intermediates, while other regions have dissimilar levels of exchange for the two species. Furthermore, as the aggregates mature into fibrils at pH 1.5, the H/D profile changes into one that is similar to those of mature fibrils at pH 2.0, pointing to a common fibril assembly process in which prefibrillar intermediates are formed first and subsequently rearrange into the final fibril structure. This observation is consistent with the nucleated conformational conversion (NCC) mechanism (90), in which monomers in solution coalesce into amorphous oligomers that later undergo reorganizations that produce ordered oligomers and finally amyloid fibrils rich in β -sheets. Indeed, the formation of amyloidogenic oligomers in the process of fibril formation at pH 2.0 has been detected and quantified by a single-molecule fluorescence study (91). The partial protection from H/D exchange in PI3-SH3 intermediates indicates a significant degree of intermolecular organization, which is preserved and extended in the mature fibrils to most residues in the A12–G29 stretch. Notably, these protected residues include the mutation-sensitive RT loop–DT segment of residues D23–L28 as well as part of the N-terminal β -strand of the fibril state. However, while the latter segment (A12–K18) is well ordered according to our MAS NMR data, several residues within the protected segment present weak NMR signals consistent with local structural disorder, namely, residues E19–I24, as described above. Therefore, while residues 12–29 are part of a highly persistent structure in the oligomeric intermediates that drive the initial steps of fibril formation and remain within the core of mature fibrils, our MAS NMR analysis shows that only some of them adopt a highly ordered β -sheet conformation in the final fibril state.

These observations provide further insight into the different roles that distinct segments of the PI3-SH3 sequence may play during the course of aggregation and fibril elongation. Residues 23–28 (DIDLHL) present a binary hydrophilic–hydrophobic pattern that has been shown to promote aggregation in various proteins (92, 93) and may be responsible for the coalescence of partially ordered oligomers starting from unfolded PI3-SH3 monomers. The few preceding residues [17–22 (KKEREE)], on the other hand, are hydrophilic and positively charged at pH 2.0, yet they do not interfere with aggregation and are partially protected from H/D exchange in both oligomers and fibrils. Finally, residues on both sides of the protected region form β -sheets in the fibril structure (β -strands 1 and 2 in Figure 6), including residues Y14–K17, which are already protected in the oligomeric intermediates. While there are several aggregation-prone regions in the PI3-SH3 sequence, one in particular (near the DT) seems to be particularly important in stimulating aggregation and the formation of oligomers and eventually fibrils, in a process consistent with the NCC mechanism. These initial interactions are then likely superseded by their reorganization and the formation of well-ordered β -sheets throughout the remainder of the sequence, as revealed by the MAS NMR measurements presented here.

Implications for a Structural Model. The MAS NMR analysis described above confirms that PI3-SH3 fibrils contain extensive regions of β -structure, as do fibrils associated with degenerative or infectious diseases. In early studies, analysis of FT-IR (19) and cryo-EM data (20) has indicated that approximately some 40% of the PI3-SH3 protein sequence is contained within the fibril β -sheet core, while the remainder of the protein sequence was proposed to form connecting loops and turns

within the fibril structure (19). This picture is broadly consistent with our results that indicate that up to 55% of the PI3-SH3 peptide chain is likely to be in well-structured, predominantly β -strand conformations, although the fraction that adopts the cross- β structure characteristic of amyloid fibrils could be somewhat lower.

Our site-specific secondary structure assignments for PI3-SH3 fibrils are in good agreement with previous H/D exchange experiments, which show that most of the amide hydrogen atoms in the fibril structure are significantly protected from solvent exchange (23). Although certain regions of the PI3-SH3 polypeptide chain in the fibril, such as charged side-chain residues, show evidence of limited dynamics, the absence of segments with liquidlike motions is consistent with a compact structure, and with the finding that none of the sequence is susceptible to ready degradation by proteolytic enzymes in the fibril state (22). Thus, we can infer that, while the well-structured regions of PI3-SH3 form the core amyloid structure and rigid loops, the remaining segments of the peptide backbone are also packed tightly within the quaternary structure of the fibril.

These results, in combination with structural information for PI3-SH3 previously obtained by cryo-EM, allow us to propose a structural model for PI3-SH3 that describes a possible arrangement of the subunit strands within the fibril core. However, we wish to emphasize that this model requires validation and needs to be refined with additional structural constraints, specifically, interatomic distances and torsion angles that are presently in progress. Nevertheless, we can suggest a possible arrangement of the protein subunits within the fibril architecture given the following facts. (1) Cryo-EM data show that the width of the protofilaments composing the fibrils is ~ 20 Å, sufficient to accommodate two β -sheets, while X-ray diffraction data suggest that the sheet spacing is 9.4 Å (13, 20). The fibril cross section according to cryo-EM consists of four areas of highest electron density that have been interpreted as the positions of the β -sheets forming the fibril core, while areas of diffuse electron density form a ringlike structure and have been interpreted as arising from less ordered parts of the fibrils. (2) No peak doubling is observed in our NMR spectra, indicating that all subunits must reside in identical environments, with the lowest-symmetry axis for two sheets being a C_2 axis. (3) H/D exchange measurements show that the C-terminus has a slightly higher exchange rate compared to the rest of the sequence in the fibrils (80), which is consistent with our observation of a disordered C-terminus. (4) A tandem repeat of PI3-SH3 has been observed to form fibrils with a macroscopic morphology similar to those formed by the single-domain protein, but apparently composed of two laterally aligned protofilaments (94).

Analyzing the structural data currently available from models of amyloid fibrils (32, 95, 96), we estimated different averages for the length per residue of the β -strands, between ~ 3.2 Å/residue for straight β -strands and ~ 2.2 Å/residue for curved β -strands (see the Supporting Information). For PI3-SH3 fibrils, three sections of β -strands composed of ~ 16 residues are predicted by our chemical shift analysis. We note that these lengths are greater than those of most β -strands that typically contain up to ~ 10 residues in soluble proteins. With a lower and upper length limit of 2.2–3.2 Å/residue, the individual β -strands would be between 35 and 51 Å long. However, because chemical shift analysis is only approximate, addition of structural constraints could result in shorter β -strands in a calculated NMR structure. Cryo-EM data show a distance of ~ 42 Å between the regions of highest electron density in the fibril cross section, which may correspond to the location of tightly packed β -sheets. This leads to the

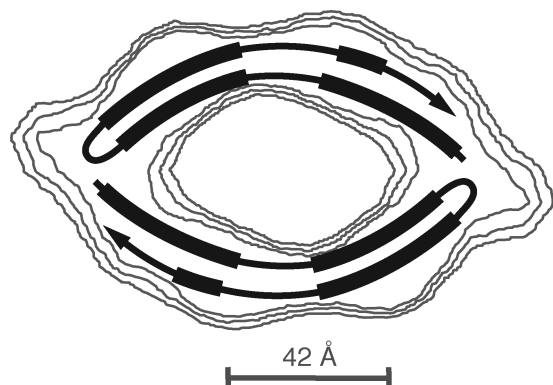


FIGURE 8: Possible model for PI3-SH3 amyloid fibril architecture. The polypeptide chains are shown as single lines, with the thick segments denoting β -sheets running into the plane of the page, and are superimposed onto the cryo-EM map (adapted from ref 20) so that each protein subunit occupies one-half of the fibril cross section. An arrowhead indicates the C-terminus.

suggestion that in the case of PI3-SH3 fibrils the β -strands in the fibril core may be arranged in long arches across the fibril cross section. These qualitative constraints then provide a limit in the number of possible arrangements, with one possibility depicted in Figure 8. In this illustration, four β -sheets form the core of two distinct protofilaments, while lateral interactions between subunits in adjacent protofilaments bring them together to form the fibrils. Further experimental data and analysis from both cryo-EM and NMR experiments will enable this and other models to be tested and suitably modified and refined.

CONCLUSIONS

The success of our MAS NMR experiments in achieving almost complete assignment of ^{13}C and ^{15}N resonances of PI3-SH3 in the amyloid fibril state, along with the identification of the majority of backbone torsion angles, suggests that a complete solid-state NMR structure of PI3-SH3 amyloid fibrils is within reach. As an alternative route, combination of our initial results with further analysis of chemical shifts (97) and cryo-EM data may lead to a detailed molecular description of the structure of a natively stable protein after conversion into the generic amyloid state, but even prior to a full structure, the data presented here have provided key information about the local conformation adopted by PI3-SH3 in amyloid fibril form. Solid-state NMR measurements have revealed a high degree of molecular organization in the amyloid fibril and shown how its secondary structure elements differ from those in the native state. Our observations for PI3-SH3 reinforce the idea that the main-chain preferences for a given type of secondary structure in the native state are not sufficient to determine those of the fibrillar state; instead, intermolecular and quaternary interactions must guide the conformation of a protein as it is incorporated in amyloid fibrils. The identification of the backbone conformation of PI3-SH3 in the fibril state has allowed us to interpret the results of previous mechanistic studies in terms of site-specific molecular structure and propose a model of protofilament assembly, thus contributing to the improved understanding of the complex mechanism of fibril formation by a natively folded protein.

ACKNOWLEDGMENT

We acknowledge stimulating conversations with Patrick van der Wel, Galia Debelouchina, Vikram Bajaj, Gaël de

Paëpe, Astrid Sivertsen, Matthew Eddy, Jozef Lewandowski, Marc Caporini, and Michele Vendruscolo.

SUPPORTING INFORMATION AVAILABLE

Two-dimensional ^{13}C – ^{13}C and ^{15}N – ^{13}C correlation spectra with complete resonance assignments, chemical shift analysis, detailed TALOS results, images of Protein Data Bank structures of amyloid fibrils mentioned above, and a chemical shift table. This material is available free of charge via the Internet at <http://pubs.acs.org>.

REFERENCES

- Chiti, F., and Dobson, C. M. (2006) Protein misfolding, functional amyloid, and human disease. *Annu. Rev. Biochem.* 75, 333–366.
- Sipe, J. D. (1992) Amyloidosis. *Annu. Rev. Biochem.* 61, 947–975.
- Sunde, M., and Blake, C. C. (1998) From the globular to the fibrous state: Protein structure and structural conversion in amyloid formation. *Q. Rev. Biophys.* 31, 1–39.
- Chiti, F., and Dobson, C. M. (2009) Amyloid formation by globular proteins under native conditions. *Nat. Chem. Biol.* 5, 15–22.
- Sacchetti, J. C., and Kelly, J. W. (2002) Therapeutic Strategies for Human Amyloid Diseases. *Nat. Rev. Drug Discovery* 1, 267–275.
- Dobson, C. M. (2003) Protein folding and misfolding. *Nature* 426, 884–890.
- Si, K., Lindquist, S., and Kandel, E. R. (2003) A neuronal isoform of the apyria CPEB has prion-like properties. *Cell* 115, 879–891.
- Coustou, V., Deleu, C., Saupe, S., and Begueret, J. (1997) The protein product of the het-s heterokaryon incompatibility gene of the fungus *Podospora anserina* behaves as a prion analog. *Proc. Natl. Acad. Sci. U.S.A.* 94, 9773–9778.
- Chapman, M. R., Robinson, L. S., Pinkner, J. S., Roth, R., Heuser, J., Hammar, M., Normark, S., and Hultgren, S. J. (2002) Role of *Escherichia coli* curli operons in directing amyloid fiber formation. *Science* 295, 851–855.
- Berson, J. F., Theos, A. C., Harper, D. C., Tenza, D., Raposo, G., and Marks, M. S. (2003) Proprotein convertase cleavage liberates a fibrillogenic fragment of a resident glycoprotein to initiate melanosome biogenesis. *J. Cell Biol.* 161, 521–533.
- Knowles, T. P., Fitzpatrick, A. W., Meehan, S., Mott, H. R., Vendruscolo, M., Dobson, C. M., and Welland, M. E. (2007) Role of intermolecular forces in defining material properties of protein nanofibrils. *Science* 318, 1900–1903.
- Uversky, V. N., and Fink, A. L. (2004) Conformational constraints for amyloid fibrillation: The importance of being unfolded. *Biochim. Biophys. Acta* 1698, 131–153.
- Guijarro, J. I., Sunde, M., Jones, J. A., Campbell, I. D., and Dobson, C. M. (1998) Amyloid Fibril Formation by an SH3 Domain. *Proc. Natl. Acad. Sci. U.S.A.* 95, 4224–4228.
- Liang, J., Chen, J. K., Schreiber, S. T., and Clardy, J. (1996) Crystal structure of PI3K SH3 domain at 2.0 angstroms resolution. *J. Mol. Biol.* 257, 632–643.
- Booker, G. W., Gout, I., Downing, A. K., Driscoll, P. C., Boyd, J., Waterfield, M. D., and Campbell, I. D. (1993) Solution structure and ligand-binding site of the SH3 domain of the p85 α subunit of phosphatidylinositol 3-kinase. *Cell* 73, 813–822.
- Koyama, S., Yu, H., Dalgarno, D. C., Shin, T. B., Zydowsky, L. D., and Schreiber, S. L. (1993) Structure of the PI3K SH3 domain and analysis of the SH3 family. *Cell* 72, 945–952.
- Koyama, S., Yu, H., Dalgarno, D., Shin, T., Zydowsky, L., and Schreiber, S. (1993) ^1H and ^{15}N assignments and secondary structure of the PI3K SH3 domain. *FEBS Lett.* 324, 93–98.
- Ahn, H. C., Le, Y. T., Nagchowdhuri, P. S., Derose, E. F., Putnam-Evans, C., London, R. E., Markley, J. L., and Lim, K. H. (2006) NMR characterizations of an amyloidogenic conformational ensemble of the PI3K SH3 domain. *Protein Sci.* 15, 2552–2557.
- Zurdo, J., Guijarro, J. I., and Dobson, C. M. (2001) Preparation and characterization of purified amyloid fibrils. *J. Am. Chem. Soc.* 123, 8141–8142.
- Jimenez, J., Guijarro, J., Orlova, E., Zurdo, J., Dobson, C., Sunde, M., and Saibil, H. (1999) Cryo-electron microscopy structure of an SH3 amyloid fibril and model of the molecular packing. *EMBO J.* 18, 815–821.
- Zurdo, J., Guijarro, J. I., Jimenez, J. L., Saibil, H. R., and Dobson, C. M. (2001) Dependence on solution conditions of aggregation and amyloid formation by an SH3 domain. *J. Mol. Biol.* 311, 325–340.

22. Polverino de Laureto, P., Taddei, N., Frare, E., Capanni, C., Costantini, S., Zurdo, J., Chiti, F., Dobson, C. M., and Fontana, A. (2003) Protein aggregation and amyloid fibril formation by an SH3 domain probed by limited proteolysis. *J. Mol. Biol.* 334, 129–141.
23. Carulla, N., Caddy, G. L., Hall, D. R., Zurdo, J., Gairi, M., Feliz, M., Giralt, E., Robinson, C. V., and Dobson, C. M. (2005) Molecular recycling within amyloid fibrils. *Nature* 436, 554–558.
24. Sunde, M., Serpell, L. C., Bartlam, M., Fraser, P. E., Pepys, M. B., and Blake, C. C. (1997) Common core structure of amyloid fibrils by synchrotron X-ray diffraction. *J. Mol. Biol.* 273, 729–739.
25. Serpell, L. C., Sunde, M., Benson, M. D., Tennent, G. A., Pepys, M. B., and Fraser, P. E. (2000) The protofilament substructure of amyloid fibrils. *J. Mol. Biol.* 300, 1033–1039.
26. Harper, J. D., Lieber, C. M., and Lansbury, P. T., Jr. (1997) Atomic force microscopic imaging of seeded fibril formation and fibril branching by the Alzheimer's disease amyloid- β protein. *Chem. Biol.* 4, 951–959.
27. Rienstra, C. M., Tucker-Kellogg, L., Jaroniec, C. P., Hohwy, M., Reif, B., McMahon, M. T., Tidor, B., Lozano-Perez, T., and Griffin, R. G. (2002) De novo determination of peptide structure with solid-state magic-angle spinning NMR spectroscopy. *Proc. Natl. Acad. Sci. U.S.A.* 99, 10260–10265.
28. Castellani, F., van Rossum, B., Diehl, A., Schubert, M., Rehbein, K., and Oschkinat, H. (2002) Structure of a protein determined by solid-state magic-angle-spinning NMR spectroscopy. *Nature* 420, 98–102.
29. Zech, S. G., Wand, A. J., and McDermott, A. E. (2005) Protein structure determination by high-resolution solid-state NMR spectroscopy: Application to microcrystalline ubiquitin. *J. Am. Chem. Soc.* 127, 8618–8626.
30. Loquet, A., Bardiaux, B., Gardienet, C., Blanchet, C., Baldus, M., Nilges, M., Malliavin, T., and Bockmann, A. (2008) 3D Structure Determination of the Crh Protein from Highly Ambiguous Solid-State NMR Restraints. *J. Am. Chem. Soc.* 130, 3579–3589.
31. Jaroniec, C. P., MacPhee, C. E., Astrof, N. S., Dobson, C. M., and Griffin, R. G. (2002) Molecular conformation of a peptide fragment of transthyretin in an amyloid fibril. *Proc. Natl. Acad. Sci. U.S.A.* 99, 16748–16753.
32. Jaroniec, C. P., MacPhee, C. E., Bajaj, V. S., McMahon, M. T., Dobson, C. M., and Griffin, R. G. (2004) High-resolution molecular structure of a peptide in an amyloid fibril determined by magic angle spinning NMR spectroscopy. *Proc. Natl. Acad. Sci. U.S.A.* 101, 711–716.
33. Heise, H., Hoyer, W., Becker, S., Andronesi, O. C., Riedel, D., and Baldus, M. (2005) Molecular-level secondary structure, polymorphism, and dynamics of full-length α -synuclein fibrils studied by solid-state NMR. *Proc. Natl. Acad. Sci. U.S.A.* 102, 15871–15876.
34. Balbach, J. J., Ishii, Y., Antzutkin, O. N., Leapman, R. D., Rizzo, N. W., Dyda, F., Reed, J., and Tycko, R. (2000) Amyloid fibril formation by A β 16–22, a seven-residue fragment of the Alzheimer's β -amyloid peptide, and structural characterization by solid state NMR. *Biochemistry* 39, 13748–13759.
35. Antzutkin, O. N., Leapman, R. D., Balbach, J. J., and Tycko, R. (2002) Supramolecular structural constraints on Alzheimer's β -amyloid fibrils from electron microscopy and solid-state nuclear magnetic resonance. *Biochemistry* 41, 15436–15450.
36. Petkova, A. T., Leapman, R. D., Guo, Z., Yau, W. M., Mattson, M. P., and Tycko, R. (2005) Self-propagating, molecular-level polymorphism in Alzheimer's β -amyloid fibrils. *Science* 307, 262–265.
37. Paravastu, A. K., Petkova, A. T., and Tycko, R. (2006) Polymorphic fibril formation by residues 10–40 of the Alzheimer's β -amyloid peptide. *Biophys. J.* 90, 4618–4629.
38. Petkova, A. T., Yau, W. M., and Tycko, R. (2006) Experimental constraints on quaternary structure in Alzheimer's β -amyloid fibrils. *Biochemistry* 45, 498–512.
39. van der Wel, P. C. A., Lewandowski, J. R., and Griffin, R. G. (2007) Solid-State NMR Study of Amyloid Nanocrystals and Fibrils Formed by the Peptide GNNQQNY from Yeast Prion Protein Sup35p. *J. Am. Chem. Soc.* 129, 5117–5130.
40. Debelouchina, G. T., Platt, G. W., Bayro, M. J., Radford, S. E., and Griffin, R. G. (2010) Magic angle spinning NMR analysis of β 2-microglobulin amyloid fibrils in two distinct morphologies. *J. Am. Chem. Soc.* 132, 10414–10423.
41. Siemer, A. B., Ritter, C., Ernst, M., Riek, R., and Meier, B. H. (2005) High-resolution solid-state NMR spectroscopy of the prion protein HET-s in its amyloid conformation. *Angew. Chem., Int. Ed.* 44, 2441–2444.
42. Chan, J. C., Oyler, N. A., Yau, W. M., and Tycko, R. (2005) Parallel β -sheets and polar zippers in amyloid fibrils formed by residues 10–39 of the yeast prion protein Ure2p. *Biochemistry* 44, 10669–10680.
43. Andronesi, O. C., Becker, S., Seidel, K., Heise, H., Young, H. S., and Baldus, M. (2005) Determination of membrane protein structure and dynamics by magic-angle-spinning solid-state NMR spectroscopy. *J. Am. Chem. Soc.* 127, 12965–12974.
44. Siemer, A. B., Arnold, A. A., Ritter, C., Westfeld, T., Ernst, M., Riek, R., and Meier, B. H. (2006) Observation of highly flexible residues in amyloid fibrils of the HET-s prion. *J. Am. Chem. Soc.* 128, 13224–13228.
45. Tycko, R. (2006) Molecular structure of amyloid fibrils: Insights from solid-state NMR. *Q. Rev. Biophys.* 39, 1–55.
46. Curtis-Fisk, J., Spencer, R. M., and Weliky, D. P. (2008) Native conformation at specific residues in recombinant inclusion body protein in whole cells determined with solid-state NMR spectroscopy. *J. Am. Chem. Soc.* 130, 12568–12569.
47. Sivertsen, A. C., Bayro, M. J., Belenky, M., Griffin, R. G., and Herzfeld, J. (2009) Solid-state NMR evidence for inequivalent GvpA subunits in gas vesicles. *J. Mol. Biol.* 387, 1032–1039.
48. Han, Y., Ahn, J., Concel, J., Byeon, I. L., Gronenborn, A. M., Yang, J., and Polenova, T. (2010) Solid-State NMR Studies of HIV-1 Capsid Protein Assemblies. *J. Am. Chem. Soc.* 132, 1976–1987.
49. LeMaster, D. M., and Kushlan, D. M. (1996) Dynamical mapping of *E. coli* thioredoxin via ^{13}C NMR relaxation analysis. *J. Am. Chem. Soc.* 118, 9255–9264.
50. Hong, M., and Jakes, K. (1999) Selective and extensive C-13 labeling of a membrane protein for solid-state NMR investigations. *J. Biomol. NMR* 14, 71–74.
51. Bennett, A. E., Rienstra, C. M., Auger, M., Lakshmi, K. V., and Griffin, R. G. (1995) Heteronuclear decoupling in rotating solids. *J. Chem. Phys.* 103, 6951–6958.
52. Bennett, A. E., Griffin, R. G., Ok, J. H., and Vega, S. (1992) Chemical shift correlation spectroscopy in rotating solids: Radio frequency-driven dipolar recoupling and longitudinal exchange. *J. Chem. Phys.* 96, 8624–8627.
53. Bennett, A. E., Rienstra, C. M., Griffiths, J. M., Zhen, W., Lansbury, P. T., Jr., and Griffin, R. G. (1998) Homonuclear radio frequency-driven recoupling in rotating solids. *J. Chem. Phys.* 108, 9463–9479.
54. Bayro, M. J., Ramachandran, R., Caporini, M. A., Eddy, M. T., and Griffin, R. G. (2008) Radio frequency-driven recoupling at high magic-angle spinning frequencies: Homonuclear recoupling sans heteronuclear decoupling. *J. Chem. Phys.* 128, 052321.
55. Verel, R., Ernst, M., and Meier, B. H. (2001) Adiabatic dipolar recoupling in solid-state NMR: The DREAM scheme. *J. Magn. Reson.* 150, 81–99.
56. De Paëpe, G., Bayro, M. J., Lewandowski, J., and Griffin, R. G. (2006) Broadband homonuclear correlation spectroscopy at high magnetic fields and MAS frequencies. *J. Am. Chem. Soc.* 128, 1776–1777.
57. Szeverenyi, N. M., Sullivan, M. J., and Maciel, G. E. (1982) Observation of spin exchange by two-dimensional fourier transform ^{13}C cross polarization-magic-angle spinning. *J. Magn. Reson.* 47, 462–475.
58. Bayro, M. J., Maly, T., Birkett, N. R., Dobson, C. M., and Griffin, R. G. (2009) Long-Range Correlations between Aliphatic ^{13}C Nuclei in Protein MAS NMR Spectroscopy. *Angew. Chem., Int. Ed.* 48, 5708–5710.
59. Baldus, M., Petkova, A. T., Herzfeld, J., and Griffin, R. G. (1998) Cross polarization in the tilted frame: Assignment and spectral simplification in heteronuclear spin systems. *Mol. Phys.* 95, 1197–1207.
60. Hing, A. W., Vega, S., and Schaefer, J. (1992) Transferred-echo double-resonance NMR. *J. Magn. Reson.* 96, 205–209.
61. Michal, C. A., and Jelinski, L. W. (1997) REDOR 3D: Heteronuclear distance measurements in uniformly labeled and natural abundance solids. *J. Am. Chem. Soc.* 119, 9059–9060.
62. Jaroniec, C., Filip, C., and Griffin, R. (2002) 3D TEDOR NMR Experiments for the Simultaneous Measurement of Multiple Carbon-Nitrogen Distances in Uniformly ^{13}C , ^{15}N -Labeled Solids. *J. Am. Chem. Soc.* 124, 10728–10742.
63. Morcombe, C. R., and Zilm, K. W. (2003) Chemical shift referencing in MAS solid state NMR. *J. Magn. Reson.* 162, 479–486.
64. Harris, R. K., Becker, E. D., Cabral de Menezes, S. M., Goodfellow, R., and Granger, P. (2001) NMR nomenclature. Nuclear spin properties and conventions for chemical shifts (IUPAC Recommendations 2001). *Pure Appl. Chem.* 73, 1795–1818.
65. Delaglio, F., Grzesiek, S., Vuister, G. W., Zhu, G., Pfeifer, J., and Bax, A. (1995) NMRPipe: A multidimensional spectral processing system based on UNIX pipes. *J. Biomol. NMR* 6, 277–293.
66. Wishart, D. S., and Sykes, B. D. (1994) The ^{13}C chemical-shift index: A simple method for the identification of protein secondary structure using ^{13}C chemical-shift data. *J. Biomol. NMR* 4, 171–180.

67. Zhang, H., Neal, S., and Wishart, D. S. (2003) RefDB: A database of uniformly referenced protein chemical shifts. *J. Biomol. NMR* 25, 173–195.
68. Cornilescu, G., Delaglio, F., and Bax, A. (1999) Protein backbone angle restraints from searching a database for chemical shift and sequence homology. *J. Biomol. NMR* 13, 289–302.
69. Helmus, J. J., Surewicz, K., Nadaud, P. S., Surewicz, W. K., and Jarosiewicz, C. P. (2008) Molecular conformation and dynamics of the Y145Stop variant of human prion protein in amyloid fibrils. *Proc. Natl. Acad. Sci. U.S.A.* 105, 6284–6289.
70. Igumenova, T. I., McDermott, A. E., Zilm, K. W., Martin, R. W., Paulson, E. K., and Wand, A. J. (2004) Assignments of carbon NMR resonances for microcrystalline ubiquitin. *J. Am. Chem. Soc.* 126, 6720–6727.
71. Franks, W. T., Zhou, D. H., Wylie, B. J., Money, B. G., Graesser, D. T., Frericks, H. L., Sahota, G., and Rienstra, C. M. (2005) Magic-angle spinning solid-state NMR spectroscopy of the β 1 immunoglobulin binding domain of protein G (GB1): ^{15}N and ^{13}C chemical shift assignments and conformational analysis. *J. Am. Chem. Soc.* 127, 12291–12305.
72. Bockmann, A., Lange, A., Galinier, A., Luca, S., Giraud, N., Juy, M., Heise, H., Montserret, R., Penin, F., and Baldus, M. (2003) Solid state NMR sequential resonance assignments and conformational analysis of the 2×10.4 kDa dimeric form of the *Bacillus subtilis* protein Crh. *J. Biomol. NMR* 27, 323–339.
73. Siemer, A. B., Ritter, C., Steinmetz, M. O., Ernst, M., Riek, R., and Meier, B. H. (2006) ^{13}C , ^{15}N resonance assignment of parts of the HET-s prion protein in its amyloid form. *J. Biomol. NMR* 34, 75–87.
74. Petkova, A. T., Ishii, Y., Balbach, J. J., Antzutkin, O. N., Leapman, R. D., Delaglio, F., and Tycko, R. (2002) A structural model for Alzheimer's β -amyloid fibrils based on experimental constraints from solid state NMR. *Proc. Natl. Acad. Sci. U.S.A.* 99, 16742–16747.
75. Seidel, K., Lange, A., Becker, S., Hughes, C. E., Heise, H., and Baldus, M. (2004) Protein solid-state NMR resonance assignments from (C-13, C-13) correlation spectroscopy. *Phys. Chem. Chem. Phys.* 6, 5090–5093.
76. Bayro, M. J., Huber, M., Ramachandran, R., Davenport, T. C., Meier, B. H., Ernst, M., and Griffin, R. G. (2009) Dipolar truncation in magic-angle spinning NMR recoupling experiments. *J. Chem. Phys.* 130, 114506.
77. Luca, S., Filippov, D. V., van Boom, J. H., Oschkinat, H., de Groot, H. J., and Baldus, M. (2001) Secondary chemical shifts in immobilized peptides and proteins: A qualitative basis for structure refinement under magic angle spinning. *J. Biomol. NMR* 20, 325–331.
78. Long, J. R., Sun, B. Q., Bowen, A., and Griffin, R. G. (1994) Molecular Dynamics and Magic Angle Spinning NMR. *J. Am. Chem. Soc.* 116, 11950–11956.
79. Maus, D. C., Copie, V., Sun, B., Griffiths, J. M., Griffin, R. G., Luo, S., Schrock, R. R., Liu, A. H., Seidel, S. W., Davis, W. M., and Grohmann, A. (1996) A Solid-State NMR Study of Tungsten Methyl Group Dynamics in $[\text{W}(\eta^5\text{-C}_5\text{Me}_5)\text{Me}_4][\text{PF}_6]$. *J. Am. Chem. Soc.* 118, 5665–5671.
80. Carulla, N., Zhou, M., Arimon, M., Gairi, M., Giralt, E., Robinson, C. V., and Dobson, C. M. (2009) Experimental characterization of disordered and ordered aggregates populated during the process of amyloid fibril formation. *Proc. Natl. Acad. Sci. U.S.A.* 106, 7828–7833.
81. Blake, C., and Serpell, L. (1996) Synchrotron X-ray studies suggest that the core of the transthyretin amyloid fibril is a continuous β -sheet helix. *Structure* 4, 989–998.
82. Ventura, S., Lacroix, E., and Serrano, L. (2002) Insights into the origin of the tendency of the PI3-SH3 domain to form amyloid fibrils. *J. Mol. Biol.* 322, 1147–1158.
83. Ventura, S., Zurdo, J., Narayanan, S., Parreño, M., Mangues, R., Reif, B., Chiti, F., Giannoni, E., Dobson, C. M., Aviles, F. X., and Serrano, L. (2004) Short amino acid stretches can mediate amyloid formation in globular proteins: The Src homology 3 SH3 case. *Proc. Natl. Acad. Sci. U.S.A.* 101, 7258–7263.
84. Chiti, F., Stefani, M., Taddei, N., Ramponi, G., and Dobson, C. M. (2003) Rationalization of the effects of mutations on peptide and protein aggregation rates. *Nature* 424, 805–808.
85. Buell, A. K., Tartaglia, G. G., Birkett, N. R., Waudby, C. A., Vendruscolo, M., Salvatella, X., Welland, M. E., Dobson, C. M., and Knowles, T. P. (2009) Position-dependent electrostatic protection against protein aggregation. *ChemBioChem* 10, 1309–1312.
86. Tartaglia, G. G., Pawar, A. P., Campioni, S., Dobson, C. M., Chiti, F., and Vendruscolo, M. (2008) Prediction of aggregation-prone regions in structured proteins. *J. Mol. Biol.* 380, 425–436.
87. Tartaglia, G. G., and Vendruscolo, M. (2008) The Zyggregator method for predicting protein aggregation propensities. *Chem. Soc. Rev.* 37, 1395–1401.
88. Otzen, D. E., and Oliveberg, M. (1999) Salt-induced detour through compact regions of the protein folding landscape. *Proc. Natl. Acad. Sci. U.S.A.* 96, 11746–11751.
89. Matysiaik, S., and Clementi, C. (2006) Minimalist protein model as a diagnostic tool for misfolding and aggregation. *J. Mol. Biol.* 363, 297–308.
90. Serio, T. R., Cashikar, A. G., Kowal, A. S., Sawicki, G. J., Moslehi, J. J., Serpell, L., Arnsdorf, M. F., and Lindquist, S. L. (2000) Nucleated conformational conversion and the replication of conformational information by a prion determinant. *Science* 289, 1317–1321.
91. Orte, A., Birkett, N. R., Clarke, R. W., Devlin, G. L., Dobson, C. M., and Klennerman, D. (2008) Direct characterization of amyloidogenic oligomers by single-molecule fluorescence. *Proc. Natl. Acad. Sci. U.S.A.* 105, 14424–14429.
92. West, M. W., Wang, W. X., Patterson, J., Mancias, J. D., Beasley, J. R., and Hecht, M. H. (1999) De novo amyloid proteins from designed combinatorial libraries. *Proc. Natl. Acad. Sci. U.S.A.* 96, 11211–11216.
93. Broome, B. M., and Hecht, M. H. (2000) Nature disfavors sequences of alternating polar and non-polar amino acids: Implications for amyloidogenesis. *J. Mol. Biol.* 296, 961–968.
94. Bader, R., Bamford, R., Zurdo, J., Luisi, B. F., and Dobson, C. M. (2006) Probing the mechanism of amyloidogenesis through a tandem repeat of the PI3-SH3 domain suggests a generic model for protein aggregation and fibril formation. *J. Mol. Biol.* 356, 189–208.
95. Wasmer, C., Lange, A., Van Melckebeke, H., Siemer, A. B., Riek, R., and Meier, B. H. (2008) Amyloid fibrils of the HET-s(218–289) prion form a β solenoid with a triangular hydrophobic core. *Science* 319, 1523–1526.
96. Iwata, K., Fujiwara, T., Matsuki, Y., Akutsu, H., Takahashi, S., Naiki, H., and Goto, Y. (2006) 3D structure of amyloid protofilaments of β 2-microglobulin fragment probed by solid-state NMR. *Proc. Natl. Acad. Sci. U.S.A.* 103, 18119–18124.
97. Robustelli, P., Cavalli, A., and Vendruscolo, M. (2008) Determination of protein structures in the solid state from NMR chemical shifts. *Structure* 16, 1764–1769.